Theory of nonlinear spin response: Rapid passage for very slow molecular reorientation

Larry R. Dalton,* Patrick Coffey, and Lauraine A. Dalton
Department of Chemistry, Vanderbilt University, Nashville, Tennessee 37235

Bruce H. Robinson
Department of Molecular Biology, Vanderbilt University, Nashville, Tennessee 37235

Alec D. Keith
Department of Biophysics, The Pennsylvania State University, University Park, Pennsylvania 16802
(Received 12 February 1973; revised manuscript received 16 September 1974)

Electron-spin-resonance (ESR) spectra, detected 90° out of phase with respect to the Zeeman modulation and using a saturating microwave field, are sensitive to molecular motion several orders of magnitude slower than are ordinary ESR spectra observed in phase with the modulation. A comprehensive theory of electron magnetic resonance based on an extension of the stochastic Liouville equation, explicitly including the effects of electromagnetic radiation and Zeeman modulation fields, of Markoffian motion modulating the magnetic anisotropy, and of relaxation and Heisenberg spin exchange, is presented. The theory is quite general and capable of explaining a large body of "modulation effects" in both single- and double-resonance experiments. Application to ^{15}N-labeled nitroxides is studied in detail, and a number of experimental spectra for the model system 2,2,6,6-tetramethyl-4-piperidone-1-oxyl (TANONE) in supercooled *sec*-butylbenzene are presented for comparison with theoretical results. When the eigenfunctions of the time-independent Hamiltonian are used as a basis set for computing spin matrix elements, pseudosecular transitions (simultaneous electron and nuclear spin flips) are found to make an important contribution to the computed spectrum in the slow tumbling region. While the out-of-phase dispersion at the first harmonic of the Zeeman modulation and the out-of-phase absorption at the second harmonic are both sensitive to slow motion, arguments based on saturation and modulation behavior favor the former as the more sensitive; greater signal-to-noise sensitivity should in fact be possible than for the ordinary ESR signal for the study of very slowly tumbling molecules.

I. INTRODUCTION

The study of electron-spin-resonance (ESR) line shapes has proved a valuable tool for investigating rotational diffusion.[1-10] A magnetically anisotropic spin-labeled compound[3-10] has its resonance condition modulated by molecular reorientation changing the orientation of magnetic tensors relative to the applied dc field. At fast correlation times ($\tau_2 \simeq 10^{-11}$ sec) the normal ESR signal (the absorption signal at the first harmonic of the modulation in phase with the modulation; recorded with a nonsaturating microwave field such that the signal changes in a linear manner with changing microwave power) shows only the isotropic g- and A-tensor components, since the anisotropic components have been averaged by rapid tumbling. As the correlation time increases, the spectrum asymptotically approaches the rigid powder spectrum arising from a fixed random orientational distribution. Although the line shape is in principle sensitive to any motion, in practice the normal ESR signal is largely insensitive to motion significantly slower than the inverse of the magnetic anisotropy, giving approximately 3×10^{-7} sec as the useful lower limit for nitroxide spin labels.

Nonlinear methods (methods which employ a saturating microwave field such that the change in signal is no longer linear with microwave power) are sensitive to much slower motion. Modulated and phase-detected saturation-transfer ESR (rapid passage), in which one monitors either the first harmonic of the dispersion or the second harmonic of the absorption signal, 90° out of phase with the Zeeman modulation field, shows sensitivity to molecular motion down to 10^{-3} sec. The rapid-passage techniques, along with electron-electron double-resonance (ELDOR) techniques, are critically dependent upon radiation and modulation fields and upon relaxation and spectral diffusion effects. While normal or linear spin-response ESR signals may be successfully simulated, ignoring interactions which induce, dissipate, or modulate saturation, investigation of nonlinear techniques absolutely requires their consideration. We recently presented an approximate but powerful simulation algorithm including these effects.[11] By neglecting pseudosecular terms (simultaneous electron and nuclear spin flips), Heisenberg spin exchange, and nuclear relaxation, we were able to treat each nuclear spin state separately, giving qualitatively accurate simulations of both linear and nonlinear spectra. We have included these

effects in the present work, and have tested the method by simulating a number of ^{15}N nitroxide spectra. ^{15}N has nuclear spin quantum number $I=\frac{1}{2}$, so that the total electron spin response is divided between only two nuclear states rather than among three, as in ^{14}N. This, along with greater magnetic moment, makes ^{15}N a more sensitive label than ^{14}N.

II. THEORY

As discussed in previous communications,[11-14] we write the equation for time evolution of the spin density matrix as

$$\frac{d\sigma(\Omega,t)}{dt}=-i\,[\mathcal{H}(\Omega,t),\sigma(\Omega,t)] - \Gamma_{\Omega}[\sigma(\Omega,t)-\sigma^{0}(\Omega,t)]. \tag{1}$$

Ω represents all orientation variables; $\mathcal{H}(\Omega,t)$ is the time-dependent spin Hamiltonian; Γ_{Ω} is a time-independent Markoff operator; and $\sigma^{0}(\Omega,t)$ is the equilibrium-spin-density matrix. For isotropic Brownian diffusion, the model used in this work, $-\Gamma_{\Omega}=D\nabla^{2}$, where D is a diffusion coefficient and ∇^{2} is the angular portion of the Laplacian operator. D is related to the correlation time as $D=1/6\tau_{2}$.

We have assumed axial symmetry for the magnetic anisotropy; this leads to a much simpler spin Hamiltonian, allowing the motional dependence to be expressed in terms of spherical harmonics rather than Wigner rotation matrices. We separate the spin Hamiltonian as

$$\mathcal{H}(\Omega,t)=\mathcal{H}_{0}+\mathcal{H}_{1}(\Omega)+\epsilon(t)+\mathcal{H}_{\mathcal{R}}\ . \tag{2}$$

$\mathcal{H}_{0}$ is the time- and orientation-independent spin Hamiltonian, including isotropic electronic and nuclear Zeeman and isotropic hyperfine interactions; $\mathcal{H}_{1}(\Omega)$ includes the anisotropic magnetic interactions modulated by molecular motion; $\epsilon(t)$ contains terms expressing the interaction of the spin system with the applied radiation and modulation fields; and $\mathcal{H}_{\mathcal{R}}$ accounts for the coupling of the spin system to the lattice. Assuming axial symmetry, $\mathcal{H}_{0}$, $\mathcal{H}_{1}(\Omega)$, and $\epsilon(t)$ for a single-resonance ESR experiment may be written as

$$\mathcal{H}_{0}=(g\beta_{e}/\hbar)H_{0}S_{z}-\gamma_{n}H_{0}I_{z}-\gamma_{e}\bar{A}S_{z}I_{z}\ , \tag{3}$$

$$\mathcal{H}_{1}(\Omega)=(\tfrac{4}{5}\pi)^{1/2}\{[\,Y_{0}^{2}(\Omega)S_{z}(F_{0}+A'I_{z}) + (Y_{1}^{2}(\Omega)I_{+}-Y_{-1}^{2}(\Omega)I_{-})S_{z}A]\}, \tag{4}$$

$$\epsilon(t)=d_{0}(S_{+}e^{-i\omega_{0}t}+S_{-}e^{i\omega_{0}t}) + (d_{s}S_{z}+d_{s}'I_{z})(e^{i\omega_{s}t}+e^{-i\omega_{s}t})\ , \tag{5}$$

where γ_{e} and γ_{n} are the electronic and nuclear gyromagnetic ratios, $\bar{A}$ is the isotropic hyperfine coupling constant, H_{0} is the static applied dc field, $F_{0}=2(g_{\parallel}-g_{\perp})\beta H_{0}/3\hbar$, $A=-2\pi(A_{\parallel}-A_{\perp})/(6)^{1/2}$, $A'=\frac{4}{3}\pi(A_{\parallel}-A_{\perp})$, $d_{0}=\frac{1}{2}\gamma_{e}h_{0}$, $d_{s}=\frac{1}{2}\gamma_{e}H_{s}$, and $d_{s}'=-\frac{1}{2}\gamma_{n}H_{s}$. H_{s} is the modulation field and h_{0} is the observing microwave field. The commutator of $\mathcal{H}_{\mathcal{R}}$ with $\sigma(\Omega,t)$ may be approximated as

$$-i\,[\mathcal{H}_{\mathcal{R}},\sigma]=-\Gamma_{\mathcal{R}}(\sigma-\sigma^{0})\ . \tag{6}$$

In the high-temperature approximation, neglecting the contribution from $\mathcal{H}_{1}(\Omega)$, σ^{0} is

$$\sigma^{0}=\rho_{0}[N^{-1}-q\mathcal{H}_{0}]\ , \tag{7}$$

where ρ_{0} is the equilibrium orientation distribution, N is the number of spin states, and $q=\hbar/NkT$. We normalize so that $\rho^{0}=Y_{0}^{0}(\Omega)$. The diagonal elements of $\Gamma_{\mathcal{R}}$ are spin-lattice relaxation times, while the off-diagonal elements are spin-spin relaxation times.

It is important to note that relaxation is to the equilibrium spin-density matrix. We actually wish to solve not for σ, but rather for $\chi\equiv\sigma-\sigma^{0}$, the deviation from equilibrium. The matrix elements of χ can readily be calculated using the eigenfunctions of $\mathcal{H}_{0}$ as a basis set. We then expand each element χ in a complete set of orthonormal functions. Off-diagonal elements of χ are expanded as

$$\chi_{\alpha\alpha'}^{\nu\nu'}=\sum_{n,k,j,m}C_{m}^{j}(n,k)\,Y_{m}^{j}(\Omega)\exp[\,i(n\omega_{0}\pm k\omega_{s})t\,], \tag{8}$$

while differences of diagonal elements are expanded as

$$\chi_{\alpha\alpha}^{\nu\nu}-\chi_{\alpha'\alpha'}^{\nu\nu}=\sum_{n,k,j,m}B_{m}^{j}(n,k)\,Y_{m}^{j}(\Omega) \times\exp[\,i(n\omega_{0}\pm k\omega_{s})t\,], \tag{9}$$

where α and α' refer to electronic spin states and ν and ν' to nuclear spin states. Since the spherical harmonics are eigenfunctions of ∇^{2}, this expansion is particularly suitable for Brownian diffusion. For isotropic motional models, the detected signal consists only of the $j=0$ component. With phase-sensitive detection the spectrum is of the form

$$\sum_{\nu}\int_{0}^{2\pi/\omega_{s}}\{C_{0}^{0}(\nu,1,r)\exp[\,i(\omega_{0}\pm r\omega_{s})t]+C_{0}^{0*}(\nu,1,-r)\exp[-i(\omega_{0}\mp r\omega_{s})t\,]\} \times\{V(H_{s})f[\cos\omega_{0}t\cos(r\omega_{s}t+\phi)\text{ or }\sin\omega_{0}t\cos(r\omega_{s}t+\phi)]\}\,dt\ . \tag{10}$$

The first term is the coherent response of the spin system, while the second term is a reference signal used to select a given Fourier component. The coherent response involves only the $j=0$, $m=0$ component; our interest in other j and m components is only in their coupling to $j=0$, $m=0$. The additional index ν in Eq. (10) refers to the matrix element that has been expanded. The summation is over only secular (electron-flip-only) transitions.

Application to ^{15}N nitroxide spectra is straightforward. Diagrams of the different ^{15}N levels, induced transitions, and relaxation and exchange paths are given in Fig. 1. We neglect the pure nuclear transitions 5 and 6 of Fig. 1. The close agreement between experimental and simulated spectra presented in this work supports this approximation in the weak-saturation region (before the maximum in the saturation curve). We have yet to test this approximation using very strong radiation fields.

Using the spin Hamiltonian of Eqs. (2)–(5), the off-diagonal elements of χ that are of interest are

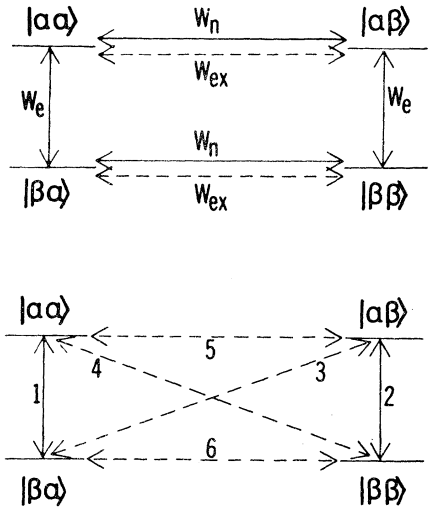

FIG. 1. Spin-lattice and Heisenberg spin exchange paths (above) and induced transitions (below) for ^{15}N. W_e and W_n refer to electronic and nuclear spin-lattice relaxation, respectively, and W_{ex} refers to Heisenberg spin exchange. The notation $|\mu\nu\rangle$ refers to electron spin state μ and nuclear spin state ν.

Transition 1.

$$\dot{\chi}^{\alpha\alpha}_{\beta\alpha} = i\{[\omega_e - \gamma_e \tfrac{1}{2}\bar{A} + d_s(e^{i\omega_s t} + e^{-i\omega_s t}) + (\tfrac{4}{5}\pi)^{1/2} Y_0^2(\Omega)(F_0 + \tfrac{1}{2}A')]\chi^{\alpha\alpha}_{\beta\alpha} + d_0 e^{i\omega_0 t}((\chi^{\alpha\alpha}_{\beta\beta} - \chi^{\alpha\alpha}_{\alpha\alpha}) + q[\omega_e - \gamma_e \tfrac{1}{2}\bar{A}]\rho^0) - \tfrac{1}{2}(\tfrac{4}{5}\pi)^{1/2} A[\chi^{\alpha\beta}_{\beta\alpha} Y^2_{-1}(\Omega) - \chi^{\beta\alpha}_{\beta\alpha} Y^2_1(\Omega)]\} - \Gamma_{\mathcal{R}}\chi^{\alpha\alpha}_{\beta\alpha} + D\nabla^2\chi^{\alpha\alpha}_{\beta\alpha}, \tag{11}$$

Transition 2.

$$\dot{\chi}^{\beta\beta}_{\beta\alpha} = i\{[\omega_e + \gamma_e \tfrac{1}{2}\bar{A} + d_s(e^{i\omega_s t} + e^{-i\omega_s t}) + (\tfrac{4}{5}\pi)^{1/2} Y_0^2(\Omega)(F_0 - \tfrac{1}{2}A')]\chi^{\beta\beta}_{\beta\alpha} + d_0 e^{i\omega_0 t}((\chi^{\beta\beta}_{\beta\beta} - \chi^{\beta\beta}_{\alpha\alpha}) + q[\omega_e + \gamma_e \tfrac{1}{2}\bar{A}]\rho^0) - \tfrac{1}{2}(\tfrac{4}{5}\pi)^{1/2} A[\chi^{\alpha\beta}_{\beta\alpha} Y^2_{-1}(\Omega) - \chi^{\beta\alpha}_{\beta\alpha} Y^2_1(\Omega)]\} - \Gamma_{\mathcal{R}}\chi^{\beta\beta}_{\beta\alpha} + D\nabla^2\chi^{\beta\beta}_{\beta\alpha}, \tag{12}$$

Transition 3.

$$\dot{\chi}^{\alpha\beta}_{\beta\alpha} = i\{[\omega_e + \omega_n + (d_s - d_s')(e^{i\omega_s t} + e^{-i\omega_s t}) + (\tfrac{4}{5}\pi)^{1/2} Y_0^2(\Omega)F_0]\chi^{\alpha\beta}_{\beta\alpha} + \tfrac{1}{2}(\tfrac{4}{5}\pi)^{1/2} A Y_1^2(\Omega)(\chi^{\alpha\alpha}_{\beta\alpha} + \chi^{\beta\beta}_{\beta\alpha})\} - \Gamma_{\mathcal{R}}\chi^{\alpha\beta}_{\beta\alpha} + D\nabla^2\chi^{\alpha\beta}_{\beta\alpha}, \tag{13}$$

Transition 4.

$$\dot{\chi}^{\beta\alpha}_{\beta\alpha} = i\{[\omega_e - \omega_n + (d_s + d_s')(e^{i\omega_s t} + e^{-i\omega_s t}) + (\tfrac{4}{5}\pi)^{1/2} Y_0^2(\Omega)F_0]\chi^{\beta\alpha}_{\beta\alpha} - \tfrac{1}{2}(\tfrac{4}{5}\pi)^{1/2} A Y^2_{-1}(\Omega)(\chi^{\alpha\alpha}_{\beta\alpha} + \chi^{\beta\beta}_{\beta\alpha})\} - \Gamma_{\mathcal{R}}\chi^{\beta\alpha}_{\beta\alpha} + D\nabla^2\chi^{\beta\alpha}_{\beta\alpha}, \tag{14}$$

where ω_0 is the observer frequency, ω_e is the electronic transition frequency, and ω_n is the nuclear transition frequency. Expanding as in Eqs. (8) and (9), multiplying Eqs. (11) and (12) by $[Y_0^i(\Omega)\exp\{i(\omega_0 + r\omega_s)t\}]^*$, and integrating gives

Transition 1.

$$\{\omega_0-\omega_e+\gamma_e\tfrac{1}{2}\bar{A}+r\omega_s-i[\,T_{2e}^{-1}+Dl(l+1)]\}C_0^l(1,1,r)$$
$$=d_s[\,C_0^l(1,1,r+1)+C_0^l(1,1,r-1)]+(F_0+\tfrac{1}{2}A')(\hat{l})^{1/2}\sum_{l'}(\hat{l}')^{1/2}\begin{pmatrix}l&2&l'\\0&0&0\end{pmatrix}^2 C_0^{l'}(1,1,r)$$
$$-\tfrac{1}{2}A(\hat{l})^{1/2}\sum_{l'}(\hat{l}')^{1/2}\begin{pmatrix}l&2&l'\\0&0&0\end{pmatrix}\begin{pmatrix}l&2&l'\\0&-1&1\end{pmatrix}[C_1^{l'}(3,1,r)-C_{-1}^{l'}(4,1,r)]$$
$$+d_0\{B_0^l(1,0,r)+q[(\omega_e-\gamma_e\tfrac{1}{2}\bar{A})\delta_{l,0}\delta_{r,0}]\}\ , \tag{15}$$

Transition 2.

$$\{\omega_0-\omega_e-\gamma_e\tfrac{1}{2}\bar{A}+r\omega_s-i[\,T_{2e}^{-1}+Dl(l+1)]\}C_0^l(2,1,r)$$
$$=d_s[\,C_0^l(2,1,r+1)+C_0^l(2,1,r-1)]+(F_0-\tfrac{1}{2}A')(\hat{l})^{1/2}\sum_{l'}(\hat{l}')^{1/2}\begin{pmatrix}l&2&l'\\0&0&0\end{pmatrix}^2 C_0^{l'}(2,1,r)$$
$$-\tfrac{1}{2}A(\hat{l})^{1/2}\sum_{l'}(\hat{l}')^{1/2}\begin{pmatrix}l&2&l'\\0&0&0\end{pmatrix}^2\begin{pmatrix}l&2&l'\\0&-1&1\end{pmatrix}[C_1^{l'}(3,1,r)-C_{-1}^{l'}(4,1,r)]$$
$$+d_0\{B_0^l(2,0,r)+q[(\omega_e+\gamma_e\tfrac{1}{2}\bar{A})\delta_{l,0}\delta_{r,0}]\}\ , \tag{16}$$

where $\hat{l}=2l+1$. Because of the symmetry properties of the Wigner $3j$ symbols, summations over l' are restricted to $l'=l-2,\ l,\ l+2$. Since we are ultimately interested only in the $l=0$ component, only even l values are required. The index i in $C_m^l(i,n,r)$ now refers to the transition scheme shown in Fig. 1.

Transitions 1 and 2 couple only to the difference of the $m=1$ component of transition 3 and the $m=-1$ component of transition 4. By neglecting the nuclear Larmor frequency we may consider only this difference. Noting that $[\,Y_m^l(\Omega)]^*=(-1)^m Y_{-m}^l(\Omega)$, we get

Transition 3-Transition 4.

$$\{\omega_0-\omega_e+r\omega_s-i[\,T_{2e}^{-1}+Dl(l+1)]\}[\,C_1^l(3,1,r)-C_{-1}^l(4,1,r)]$$
$$=d_s\{[\,C_1^l(3,1,r+1)-C_{-1}^l(4,1,r+1)]+[\,C_1^l(3,1,r-1)-C_{-1}^l(4,1,r-1)]\}$$
$$-F_0(\hat{l})^{1/2}\sum_{l'}(\hat{l}')^{1/2}\begin{pmatrix}l&2&l'\\0&0&0\end{pmatrix}\begin{pmatrix}l&2&l'\\1&0&-1\end{pmatrix}[C_1^{l'}(3,1,r)-C_{-1}^{l'}(4,1,r)]$$
$$-A(\hat{l})^{1/2}\sum_{l'}(\hat{l}')^{1/2}\begin{pmatrix}l&2&l'\\0&0&0\end{pmatrix}\begin{pmatrix}l&2&l'\\1&-1&0\end{pmatrix}[C_0^{l'}(1,1,r)+C_0^{l'}(2,1,r)]\ . \tag{17}$$

In the same manner, the diagonal elements $B_0^l(1,0,r)$ and $B_0^l(2,0,r)$ may be derived as

$$\{r\omega_s-i[\,T_{1e}^{-1}+(2T_{1n})^{-1}+W_{ex}]\}B_0^l(1,0,r)$$
$$+i[(2T_{1n})^{-1}+W_{ex}]B_0^l(2,0,r)$$
$$=2d_0[\,C_0^l(1,1,r)-C_0^l{}^*(1,1,-r)]\ , \tag{18}$$
$$\{r\omega_s-i[\,T_{1e}^{-1}+(2T_{1n})^{-1}+W_{ex}]\}B_0^l(2,0,r)$$
$$+i[(2T_{1n})^{-1}+W_{ex}]B_0^l(1,0,r)$$
$$=2d_0[\,C_0^l(2,1,r)-C_0^l{}^*(2,1,-r)]\ . \tag{19}$$

We have included the nuclear spin-lattice relaxation time T_{1n} and the Heisenberg spin-exchange frequency W_{ex} in the equations for the diagonal elements. Separating the complex number $C_m^l(i,n,k)$ into a real part $C_m'^l(i,n,k)$ and an imaginary part $C_m''^l(i,n,k)$, Eqs. (15)–(19) may be rearranged in terms of the four signals

$$\begin{aligned}
&\alpha_m^l(i,1,r)\equiv C_m'^l(i,1,r)+C_m'^l(i,1,-r)\ ,\\
&\beta_m^l(i,1,r)\equiv C_m''^l(i,1,r)-C_m''^l(i,1,-r)\ ,\\
&\gamma_m^l(i,1,r)\equiv C_m''^l(i,1,r)+C_m''^l(i,1,-r)\ ,\\
&\delta_m^l(i,1,r)\equiv C_m'^l(i,1,r)-C_m'^l(i,1,-r)\ .
\end{aligned} \tag{20}$$

These are the four independent signals arising from the Fourier analysis of Eq. (10). $\alpha_m^l(i,1,r)$, $\beta_m^l(i,1,r)$, $\gamma_m^l(i,1,r)$, and $\delta_m^l(i,1,r)$ represent the l and m components of the in-phase dispersion, out-of-phase dispersion, in-phase absorption, and out-of-phase absorption at the rth harmonic

TABLE I. Elements of the matrix $\mathcal{W}_{r,l}$ [cf. Eq. (21)]. See Table IV for definition of terms.

$\Delta(1,l)$	0	$\Lambda_3(r,l)$	$\Lambda_4(r,l)$	0	0	$\Lambda_5(r,l)$	$\Lambda_6(r,l)$	$\Lambda_7(l,l)$	0	0	0
0	$\Delta(1,l)$	$\Lambda_4(r,l)$	$-\Lambda_3(r,l)$	0	0	$\Lambda_6(r,l)$	$-\Lambda_5(r,l)$	0	$\Lambda_7(l,l)$	0	0
$-\Lambda_2(l)$	$r\omega_s$	$\Delta(1,l)$	0	0	0	0	0	0	0	$\Lambda_7(l,l)$	0
$r\omega_s$	$\Lambda_2(l)$	0	$\Delta(1,l)$	0	0	0	0	0	0	0	$\Lambda_7(l,l)$
0	0	$\Lambda_5(r,l)$	$\Lambda_6(r,l)$	$\Delta(2,l)$	0	$\Lambda_3(r,l)$	$\Lambda_4(r,l)$	$\Lambda_7(l,l)$	0	0	0
0	0	$\Lambda_6(r,l)$	$-\Lambda_5(r,l)$	0	$\Delta(2,l)$	$\Lambda_4(r,l)$	$-\Lambda_3(r,l)$	0	$\Lambda_7(l,l)$	0	0
0	0	0	0	$-\Lambda_2(l)$	$r\omega_s$	$\Delta(2,l)$	0	0	0	$\Lambda_7(l,l)$	0
0	0	0	0	$r\omega_s$	$\Lambda_2(l)$	0	$\Delta(2,l)$	0	0	0	$\Lambda_7(l,l)$
$2\Lambda_7(l,l)$	0	0	0	$2\Lambda_7(l,l)$	0	0	0	$\Delta(3-4,l)$	0	$\Lambda_2(l)$	$r\omega_s$
0	$2\Lambda_7(l,l)$	0	0	0	$2\Lambda_7(l,l)$	0	0	0	$\Delta(3-4,l)$	$r\omega_s$	$-\Lambda_2(l)$
0	0	$2\Lambda_7(l,l)$	0	0	0	$2\Lambda_7(l,l)$	0	$-\Lambda_2(l)$	$r\omega_s$	$\Delta(3-4,l)$	0
0	0	0	$2\Lambda_7(l,l)$	0	0	0	$2\Lambda_7(l,l)$	$r\omega_s$	$\Lambda_2(l)$	0	$\Delta(3-4,l)$

of the modulation, respectively. The ESR spectra observed are $\alpha_0^0(1,1,r)+\alpha_0^0(2,1,r)$, $\beta_0^0(1,1,r)+\beta_0^0(2,1,r)$, $\gamma_0^0(1,1,r)+\gamma_0^0(2,1,r)$, and $\delta_0^0(1,1,r)+\delta_0^0(2,1,r)$, respectively. After considerable algebraic manipulation, and making use of the relationships $\alpha_m^l(i,1,-r)=\alpha_m^l(i,1,r)$, $\beta_m^l(i,1,-r)=-\beta_m^l(i,1,r)$, $\gamma_m^l(i,1,-r)=\gamma_m^l(i,1,r)$, and $\delta_m^l(i,1,-r)=-\delta_m^l(i,1,r)$, we write the master matrix equation as

$$\mathcal{W}_{r,l}\,\mathcal{S}_{r,l}=\mathcal{S}'_{r,l}\,, \tag{21}$$

where $\mathcal{W}_{r,l}$, $\mathcal{S}_{r,l}$, and $\mathcal{S}'_{r,l}$ are defined as in Tables I–IV.

III. INSTRUMENTATION AND EXPERIMENTAL METHODS

Measurements were performed with a Varian E-12 spectrometer equipped with absorption and dispersion reference arms (E-101-15 microwave bridge). The modulation transmitters and receivers were modified to effect improved waveform purity, improved phase isolation, and precisely variable modulation frequency.

TABLE II. Elements of the vector $\mathcal{S}_{r,l}$ [cf. Eq. (21)].

$\alpha_0^l(1,1,r)$
$\beta_0^l(1,1,r)$
$\gamma_0^l(1,1,r)$
$\delta_0^l(1,1,r)$
$\alpha_0^l(2,1,r)$
$\beta_0^l(2,1,r)$
$\gamma_0^l(2,1,r)$
$\delta_0^l(2,1,r)$
$\alpha_1^l(3,1,r)-\alpha_{-1}^l(4,1,r)$
$\beta_1^l(3,1,r)-\beta_{-1}^l(4,1,r)$
$\gamma_1^l(3,1,r)-\gamma_{-1}^l(4,1,r)$
$\delta_1^l(3,1,r)-\delta_{-1}^l(4,1,r)$

Temperature was controlled using a Varian E-257 temperature controller, and was measured using a Leeds and Northrup 8692-2 temperature potentiometer equipped with a copper-constantan thermocouple. Sample cell and Dewar insert designs were modified to prevent sample vibration under the effect of the coolant stream and to prevent the coolant gas stream from coming in contact with the microwave cavity, thereby affecting cavity tuning.

In order to compare experimental and calculated spectra, it was necessary to measure microwave and modulation field intensities. The microwave field intensity was measured as previously described.[12] Modulation field amplitudes were measured from modulation sideband separations observed with an aqueous K_2CO_3-buffered sample of potassium nitrosodisulfonate. The modulation amplitude equals the sideband separation plus the resonance linewidth. Modulation amplitudes less than the linewidth of the $m_I=0$ transition of the nitrosodisulfonate ion were measured using an oscilloscope to monitor voltage induced in a coil placed in the cavity. In order to minimize the variation of microwave and modulation fields along the sample, the sample volume was restricted to that of a cylinder approximately 3 mm in diameter and 5 mm in length.

The preparation of ^{15}N-TANONE was accomplished as follows: The piperidine synthesis of Francis[15] was scaled down and modified to accommodate feasible quantities of $^{15}NH_3$. About 0.5 ml of liquid $^{15}NH_3$ was added to 5 ml of cold acetone containing 1.6 g of $CaCl_2$. After stirring for 4 days, the resulting ^{15}N-triacetoneamine was extracted into ether and purified by thin-layer chromatography using diethyl ether as the mobile

phase on a Silica Gel G stationary phase. Triacetonamine was oxidized with perbenzoic acid to the nitroxyl free radical 2,2,6,6-tetramethyl-4-piperidone-1-oxyl (TANONE) and similarly purified by preparative thin-layer chromatography.

Spin labels were dissolved in *sec*-butylbenzene (99+%) obtained from Aldrich Chemical Co. All samples examined in this study were in the concentration range of 10^{-3}–10^{-5} *M*. Oxygen was removed from samples by careful degassing on a vacuum line employing a repetitive freeze-pump-melt technique.

Computer calculations were carried out on an XDS Sigma 7 with programs written in Fortran IV. All spectra displayed in this work required 8.5*K* words of memory and between 5 and 250 min execution time. Programs are available from the authors upon request.

IV. RESULTS AND DISCUSSION

Computer simulations for TANONE (cf. Fig. 2) based on the above equations are presented in Figs. 3–5. Figure 3 displays the normal ESR signal, the in-phase absorption at the first harmonic; Fig. 4 consists of the in-phase dispersion at the first harmonic; and Fig. 5 is the out-of-phase dispersion at the first harmonic. This last figure is an example of modulated and phase-detected saturation-transfer spectroscopy (rapid passage). The following parameters were assumed: $T_{1e}=1.0\times10^{-5}$ sec, $T_{2e}=1.6\times10^{-8}$ sec, $(2T_{1n})^{-1}+W_{ex}=5\times10^{3}$ Hz, $h_0=0.075$ G, $H_s=0.02$ G, $\omega_s=2\pi\times10^{5}$ Hz, $g_{\parallel}=2.00220$, $g_{\perp}=2.00775$, $A_{\parallel}=131.32$ MHz, $A_{\perp}=18.79$ MHz. The T_{2e} value used is not the actual T_{2e}, but has been adjusted to simulate the superhyperfine coupling of the neighboring methyl and methylene protons. Note that both the in-phase absorption and dispersion signals (Figs. 3 and 4) are relatively insensitive to changes in correlation time beyond 10^{-7} sec, while the passage signal (Fig. 5) shows marked changes down to 10^{-3} sec. Figure 6 displays four experimental passage spectra at different temperatures; the agreement between the simulated and experimental spectra is quite good, with the exception of the central region of the spectrum. The assumption of axial symmetry is much better for the *A*-tensor anisotropy than for the *g* tensor; *g*-tensor anisotropy is the dominant effect in

TABLE III. Elements of the vector $\mathcal{S}'_{r,l}$ [c.f. Eq. (21)]. The summations are over the values $l'=l+2$, $l-2$ only.

$$
\begin{bmatrix}
d_s[\alpha^l_0(1,1,r+1)+\alpha^l_0(1,1,r-1)]-\sum_{l'}\Lambda_8(l,l')\alpha^{l'}_0(1,1,r)-\sum_{l'}\Lambda_7(l,l')[\alpha^{l'}_1(3,1,r)-\alpha^{l'}_{-1}(4,1,r)]+\mathfrak{Q}_1(r,l)\\
d_s[\beta^l_0(1,1,r+1)+\beta^l_0(1,1,r-1)]-\sum_{l'}\Lambda_8(l,l')\beta^{l'}_0(1,1,r)-\sum_{l'}\Lambda_7(l,l')[\beta^{l'}_1(3,1,r)-\beta^{l'}_{-1}(4,1,r)]\\
d_s[\gamma^l_0(1,1,r+1)+\gamma^l_0(1,1,r-1)]-\sum_{l'}\Lambda_8(l,l')\gamma^{l'}_0(1,1,r)-\sum_{l'}\Lambda_7(l,l')[\gamma^{l'}_1(3,1,r)-\gamma^{l'}_{-1}(4,1,r)]\\
d_s[\delta^l_0(1,1,r+1)+\delta^l_0(1,1,r-1)]-\sum_{l'}\Lambda_8(l,l')\delta^{l'}_0(1,1,r)-\sum_{l'}\Lambda_7(l,l')[\delta^{l'}_1(3,1,r)-\delta^{l'}_{-1}(4,1,r)]\\
d_s[\alpha^l_0(2,1,r+1)+\alpha^l_0(2,1,r-1)]-\sum_{l'}\Lambda_9(l,l')\alpha^{l'}_0(2,1,r)-\sum_{l'}\Lambda_7(l,l')[\alpha^{l'}_{-1}(3,1,r)-\alpha^{l'}_{-1}(4,1,r)]+\mathfrak{Q}_2(r,l)\\
d_s[\beta^l_0(2,1,r+1)+\beta^l_0(2,1,r-1)]-\sum_{l'}\Lambda_9(l,l')\beta^{l'}_0(2,1,r)-\sum_{l'}\Lambda_7(l,l')[\beta^{l'}_1(3,1,r)-\beta^{l'}_{-1}(4,1,r)]\\
d_s[\gamma^l_0(2,1,r+1)+\gamma^l_0(2,1,r-1)]-\sum_{l'}\Lambda_9(l,l')\gamma^{l'}_0(2,1,r)-\sum_{l'}\Lambda_7(l,l')[\gamma^{l'}_1(3,1,r)-\gamma^{l'}_{-1}(4,1,r)]\\
d_s[\delta^l_0(2,1,r+1)+\delta^l_0(2,1,r-1)]-\sum_{l'}\Lambda_9(l,l')\delta^{l'}_0(2,1,r)-\sum_{l'}\Lambda_7(l,l')[\delta^{l'}_1(3,1,r)-\delta^{l'}_{-1}(4,1,r)]\\
d_s\{[\alpha^l_1(3,1,r+1)-\alpha^l_{-1}(4,1,r+1)]+[\alpha^l_1(3,1,r-1)-\alpha^l_{-1}(4,1,r-1)]\}-\sum_{l'}\Lambda_{10}(l,l')[\alpha^{l'}_1(3,1,r)-\alpha^{l'}_{-1}(4,1,r)]\\
\quad-2\sum_{l'}\Lambda_7(l,l')[\alpha^{l'}_0(1,1,r)+\alpha^{l'}_0(2,1,r)]\\
d_s\{[\beta^l_1(3,1,r+1)-\beta^l_{-1}(4,1,r+1)]+[\beta^l_1(3,1,r-1)-\beta^l_{-1}(4,1,r-1)]\}-\sum_{l'}\Lambda_{10}(l,l')[\beta^{l'}_1(3,1,r)-\beta^{l'}_{-1}(4,1,r)]\\
\quad-2\sum_{l'}\Lambda_7(l,l')[\beta^{l'}_0(1,1,r)+\beta^{l'}_0(2,1,r)]\\
d_s\{[\gamma^l_1(3,1,r+1)-\gamma^l_{-1}(4,1,r+1)]+[\gamma^l_1(3,1,r-1)-\gamma^l_{-1}(4,1,r-1)]\}-\sum_{l'}\Lambda_{10}(l,l')[\gamma^{l'}_1(3,1,r)-\gamma^{l'}_{-1}(4,1,r)]\\
\quad-2\sum_{l'}\Lambda_7(l,l')[\gamma^{l'}_0(1,1,r)+\gamma^{l'}_0(2,1,r)]\\
d_s\{[\delta^l_1(3,1,r+1)-\delta^l_{-1}(4,1,r+1)]+\{\delta^l_1(3,1,r-1)-\delta^l_{-1}(4,1,r-1)]\}-\sum_{l'}\Lambda_{10}(l,l')[\delta^{l'}_1(3,1,r)-\delta^{l'}_{-1}(4,1,r)]\\
\quad-2\sum_{l'}\Lambda_7(l,l')[\delta^{l'}_0(1,1,r)+\delta^{l'}_0(2,1,r)]
\end{bmatrix}
$$

TABLE IV. Definitions of terms in Tables I and III.

$$\Delta(1,l)=\omega_0-\omega_e+\gamma_e\tfrac{1}{2}\bar{A}-(F_0+\tfrac{1}{2}A')(\hat{l})\begin{pmatrix} l & 2 & l \\ 0 & 0 & 0\end{pmatrix}^2$$

$$\Delta(2,l)=\omega_0-\omega_e-\gamma_e\tfrac{1}{2}\bar{A}-(F_0-\tfrac{1}{2}A')(\hat{l})\begin{pmatrix} l & 2 & l \\ 0 & 0 & 0\end{pmatrix}^2$$

$$\Delta(3-4,l)=\omega_0-\omega_e+F_0(\hat{l})\begin{pmatrix} l & 2 & l \\ 0 & 0 & 0\end{pmatrix}\begin{pmatrix} l & 2 & l \\ 1 & 0 & -1\end{pmatrix}$$

$$\Lambda_1(l)=T_{1e}^{-1}+\mathfrak{R}+Dl(l+1)$$

$$\Lambda_2(l)+T_{2e}^{-1}+Dl(l+1)$$

$$\Lambda_3(r,l)=\Lambda_2(l)+\Lambda_1(l)\mathfrak{L}(r,l)[\Lambda_1^2(l)+(r\omega_s)^2-\mathfrak{R}^2]$$

$$\Lambda_4(r,l)=r\omega_s\{1-\mathfrak{L}(r,l)[\Lambda_1^2(l)+(r\omega_s)^2+\mathfrak{R}^2]\}$$

$$\Lambda_5(r,l)=-\mathfrak{L}(r,l)\mathfrak{R}[-\Lambda_1^2(l)+(r\omega_s)^2+\mathfrak{R}^2]$$

$$\Lambda_6(r,l)=-2\mathfrak{L}(r,l)\mathfrak{R}(r\omega_s)\Lambda_1(l)$$

$$\Lambda_7(l,l')=\tfrac{1}{2}A(\hat{l})^{1/2}(\hat{l}')^{1/2}\begin{pmatrix} l & 2 & l' \\ 0 & 0 & 0\end{pmatrix}\begin{pmatrix} l & 2 & l' \\ 0 & 1 & -1\end{pmatrix}$$

$$\Lambda_8(l,l')=-(F_0+\tfrac{1}{2}A')(\hat{l})^{1/2}(\hat{l}')^{1/2}\begin{pmatrix} l & 2 & l' \\ 0 & 0 & 0\end{pmatrix}^2$$

$$\Lambda_9(l,l')=-(F_0-\tfrac{1}{2}A')(\hat{l})^{1/2}(\hat{l}')^{1/2}\begin{pmatrix} l & 2 & l' \\ 0 & 0 & 0\end{pmatrix}^2$$

$$\Lambda_{10}(l,l')=F_0(\hat{l})^{1/2}(\hat{l}')^{1/2}\begin{pmatrix} l & 2 & l' \\ 0 & 0 & 0\end{pmatrix}\begin{pmatrix} l & 2 & l' \\ 1 & 0 & -1\end{pmatrix}$$

$$\mathfrak{L}(r,l)=4d_0^2/\{\Lambda_1^4(l)+(r\omega_s)^4+\mathfrak{R}^4+2[\mathfrak{R}^2(r\omega_s)^2+\Lambda_1^2(l)(r\omega_s)^2-\Lambda_1^2(l)\mathfrak{R}^2]\}$$

$$\mathfrak{R}=(2T_{1n})^{-1}+W_{ex}$$

$$\mathfrak{Q}_1(r,l)=q[(\omega_e-\gamma_e\tfrac{1}{2}\bar{A})\delta_{l,0}\delta_{r,0}]$$

$$\mathfrak{Q}_2(r,l)=q[(\omega_e+\gamma_e\tfrac{1}{2}\bar{A})\delta_{l,0}\delta_{r,0}]$$

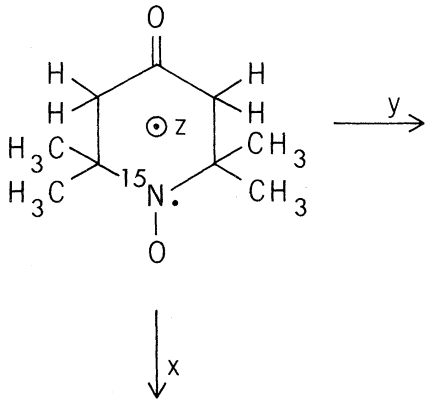

FIG. 2. Molecular structure of ^{15}N-2, 2, 6, 6-tetramethyl-4-piperidone-N-oxyl (^{15}N-TANONE) is shown with the molecular fixed-axis system indicated.

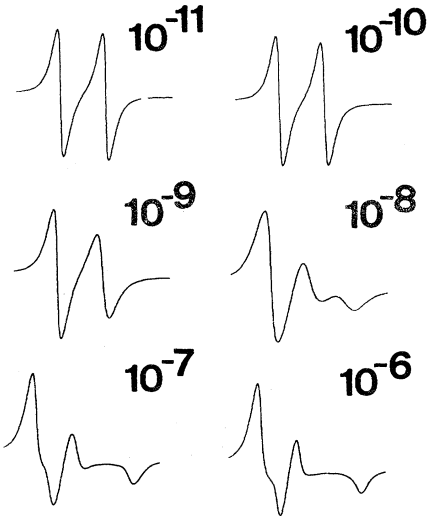

FIG. 3. Normal ESR spectra of TANONE (the in-phase absorption spectra at the first harmonic of the modulation) simulated for different correlation times, using a Brownian diffusion model. Note that the spectra are largely insensitive to changes in correlation time below $\tau_2=10^{-7}$ sec.

the central part of the spectrum. Consideration of full anisotropy requires the use of Wigner rotation matrices in $\mathfrak{K}_1(\Omega)$ rather than spherical harmonics, complicating the problem considerably.

As observed in the study of slowly tumbling spin

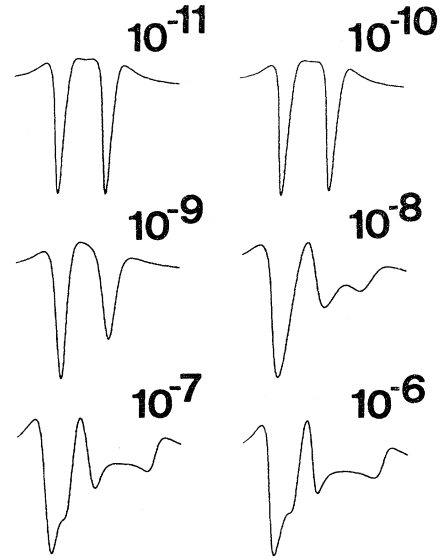

FIG. 4. Simulated in-phase dispersion spectra of TANONE, at the first harmonic of the modulation, computed employing a Brownian diffusion model. Sensitivity to molecular motion parallels the absorption spectra shown in Fig. 2.

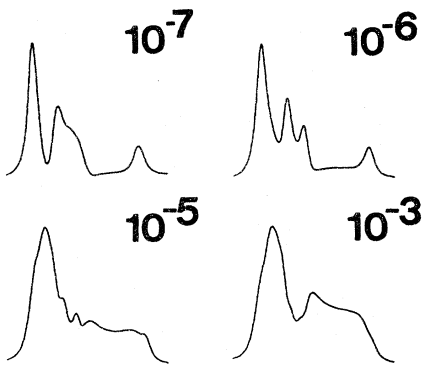

FIG. 5. Simulated rapid-passage dispersion spectra (the out-of-phase dispersion signal at the first harmonic of the modulation) for TANONE. The spectra show marked changes with changing correlation times down to $\tau_2 = 10^{-3}$ sec.

labels by ELDOR,[13] a comparison of the experimental and theoretical passage spectra suggests that in some cases free or jump diffusion models may better describe the molecular motion than does a Brownian diffusion model. This generally appears to be the case when solvent and free radical solute molecules are of comparable size; on the other hand, spin-labeled biomolecules such as maleimide-labeled hemoglobin in aqueous media appear to be well characterized by a Brownian diffusion model. We defer a detailed discussion of this point to a future publication.

The marked effects of inclusion of the pseudosecular transitions 3 and 4 of Fig. 1 can be seen in Fig. 7, where simulations including and neglecting these terms are superimposed. While trends and qualitative effects can be simulated by ignoring such transitions, quantitative simulation requires their inclusion.

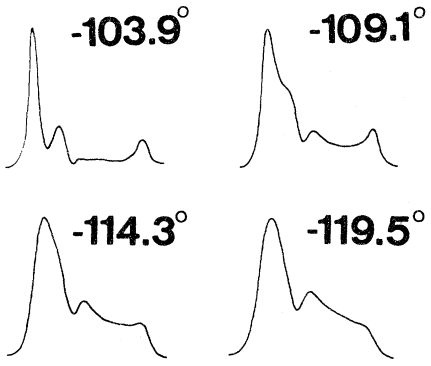

FIG. 6. Experimental rapid-passage spectra (the out-of-phase dispersion signal detected at the first harmonic of the modulation) for TANONE in *sec*-butylbenzene at different temperatures. Spectra were recorded employing a microwave observing power of 10 mW, a Zeeman modulation of 100-kHz frequency and 2.5 G peak-to-peak modulation amplitude. The spectra were recorded at the following relative gains: −103.9°, 3.1; −109.1°, 2.0; −114.3°, 1.0; −119.5°, 1.0.

Throughout this work, the value of h_0 used is in the weak-saturation region, past the linear response region of the signal-vs-microwave-power curve, but before the maximum of the curve. The dependence of the dispersion passage signal upon microwave power is demonstrated in Fig. 8. The passage signal saturates quite slowly; furthermore, biological samples in aqueous media often exhibit passage spectra that saturate even more slowly than simple nitroxides in organic solvents. We have found that maleimide-labeled oxyhemoglobin, maleimide- or iodoacetamide-labeled proteins, or nitroxide-containing lipids at ambient temperatures or lyophilized at near-ambient temperatures behave in this manner. For example, lyophilized human oxyhemoglobin yields a dispersion passage spectrum which has essentially the same line shape at 200 mW as at 20 or at 1 mW; i.e., the weak-saturation condition still obtains

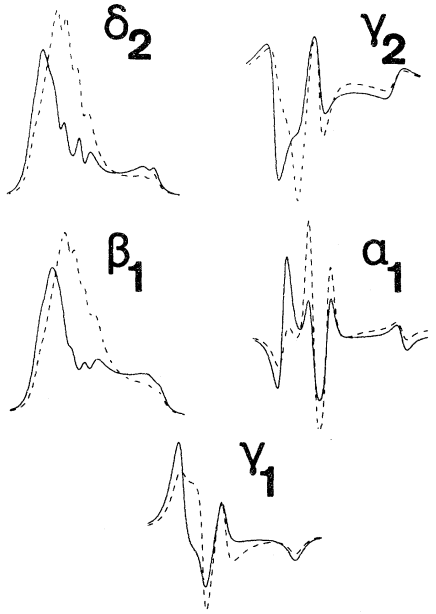

FIG. 7. Effect of including (solid lines) and neglecting (dashed lines) the pseudosecular transitions (3 and 4 of Fig. 1) in computing various in-phase and out-of-phase spectra at the first and second harmonics of the modulation. Calculations are for an isotropic Brownian diffusion model and a correlation time of 1.8×10^{-5} sec. δ_2 is the out-of-phase absorption at the second harmonic, γ_2 the in-phase absorption at the second harmonic, β_1 the out-of-phase dispersion at the first harmonic, α_1 the in-phase dispersion at the first harmonic, and γ_1 the in-phase absorption at the first harmonic.

for the highest powers available on a commercial Varian E-12 spectrometer. This observation is important for two reasons: (i) As spectral shapes are not crucially dependent upon microwave power in the weak-saturation region, the experimenter can utilize model spectra calculated under similar, but not necessarily identical, microwave field conditions to analyze spectra. The present work provides quantitative support for the initial speculation that very characteristic line shapes were observed when measuring first-harmonic dispersion[12] or second-harmonic absorption[16] passage spectra. Very simply, all early passage spectra[12,16] corresponded to the weak-saturation region. (ii) The fact that the first-harmonic dispersion passage signal saturates so slowly (more slowly than the normal ESR signal, for example) suggests that an improvement in signal-to-noise in the study of slowly tumbling spin-label systems may be realized by examining this signal. The present limiting noise source at high microwave power is klystron FM noise; there is good reason to believe that FM noise can be reduced by cavity stabilization techniques and by use of bimodal-cavity–Bloch-induction schemes for observing the dispersion signals. Examining spin-label samples in aqueous environments (using a flat cell) we calculate a limiting sensitivity of 5×10^{-7} M of nitroxide radical. As is shown in Fig. 9, the second-harmonic absorption signal saturates more quickly than the first-harmonic dispersion. We have also observed this trend in a variety of spin-labeled biological materials. For example, in lyophilized human oxyhemoglobin, line-shape changes become clearly noticeable for microwave powers between 20 and 40 mW. This difference in saturation behavior may mean that the dispersion passage signal is ultimately the more useful of the two.

Another important test of theory, and an effect relevant to the analysis of passage spectra, is the dependence of passage line shapes and signal intensities upon Zeeman modulation amplitudes. As with microwave power, we can establish two regions for the modulation field dependence. At low modulation amplitudes, the first-harmonic dispersion signal intensity increases linearly with the modulation field intensity, and the second-harmonic absorption signal increases as the square of the field intensity. In the weak-modulation region the line shape of either signal is

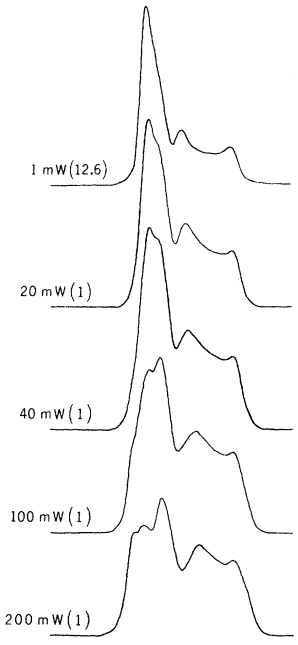

FIG. 8. Dependence of the experimental TANONE dispersion-passage spectra (out-of-phase dispersion at the frist harmonic) upon microwave power. All spectra were recorded employing a peak-to-peak modulation amplitude of 2.5 G (100-kHz modulation frequency) and the sample was maintained at a temperature of −114 °C during the measurements. The relative receiver gains employed in recording the spectra are given in parentheses following the microwave power setting.

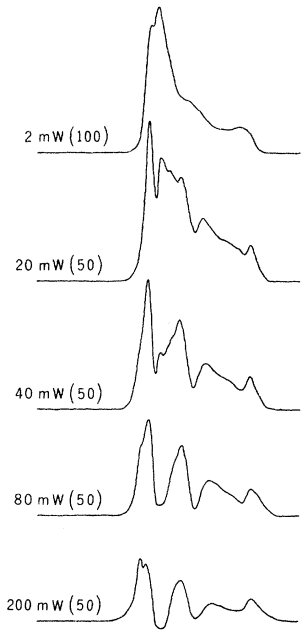

FIG. 9. Dependence of the experimental second-harmonic absorption-passage spectra (δ_2) of TANONE upon microwave power. All spectra were recorded employing a peak-to-peak modulation amplitude of 2.5 G (50-kHz modulation frequency) at a sample temperature of −114 °C. The relative receiver gains are given in parentheses.

insensitive to changing modulation amplitude. Spectra may be simulated in this region by neglecting coupling to higher modulation harmonics (r states). That is, the higher harmonics do not perturb or remodulate the lower harmonics.[17,18] The other extreme is at high modulation amplitudes, where the signal intensity no longer depends in a linear fashion upon modulation amplitude. The spectral line shape changes in this region with changing modulation amplitude (the spectra broaden and ultimately show line-splitting or sideband-splitting effects). All passage spectra published to date appear to correspond to the weak-modulation limit. For nitroxides in organic solvents and for biological samples in aqueous media, we do not observe line shapes to depend upon modulation amplitude until fields greater than 5 G are employed. A typical illustration of this point is given in Fig. 10. This result is compatible with theory, since theory predicts that line-broadening and splitting effects should not become apparent until the modulation field peak-to-peak amplitude is greater than the linewidth. There are several practical observations to be drawn from our consideration of modulation effects. First of all, one can employ larger modulation amplitudes (and hence gain signal intensity) in studying passage spectra than in studying the normal ESR spectra, since distortion effects become crucial in the latter at smaller modulation amplitudes. Since quite high modulation amplitudes can be employed without distorting passage line shapes, analysis of experimental spectra can be based on theoretical spectra calculated under similar but not identical conditions. Taken together with our observations concerning the microwave power dependence of passage spectra, this means that a single family of characteristic line shapes can be computed and will suffice for nearly all experimental situations encountered. A final consideration is that the signal intensity of the second-harmonic absorption passage signal falls off faster with decreasing modulation amplitude than does the first-harmonic dispersion signal. In practice, modulation amplitudes greater than 1 G are thus necessary for adequate signal-to-noise when examining second-harmonic signals. This observation, along with the relative microwave-power saturation behavior of the two signals, supports the desirability of the first-harmonic dispersion signal in comparison to the second-harmonic absorption.

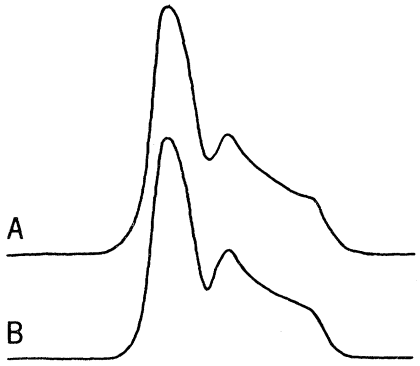

FIG. 10. Demonstration that the signal response is linear with modulation amplitude for modulation amplitude up to 2.5 G (peak-to-peak). The out-of-phase first-harmonic dispersion spectra for TANONE in *sec*-butylbenzene at −120.1 °C are shown. Spectra were recorded employing a microwave power of 10 mW and a modulation frequency of 100 kHz. Spectrum A is for a modulation amplitude of 1.0 G and a receiver gain of 250, while spectrum B is for a modulation amplitude of 2.5 G and a receiver gain of 100.

Finally, we note that the theory correctly predicts that all signal information at a given modulation harmonic is contained in the four signals α, β, γ, δ [Eq. (20)]. The response measured at an intermediate phase setting corresponds to a simple combination of two of the four signals. This follows in a straightforward manner from Eq. (10), using simple trigonometric identities.

ACKNOWLEDGMENTS

One of us (L.R.D.) wishes to acknowledge stimulating discussions with Professor Walter Gordy of Duke University at the Third Southeastern Magnetic Resonance Conference. L.R.D. also wishes to thank Professor Daniel Kivelson and Professor Mostafa El-Sayed for many stimulating discussions and kind hospitality shown him while a visiting scholar at UCLA during January 1973, when the major portion of this work was completed. The comments and private communication of results by Professor H. M. McConnell, Professor A. L. Kwiram, Dr. J. S. Hyde, and D. D. Thomas are appreciated.

Acknowledgment is made to the Donors of The Petroleum Research Fund, administered by the Americal Chemical Society, for support of this research.

*Alfred P. Sloan Foundation Fellow; author to whom correspondence should be addressed.
[1]L. T. Muus and P. W. Atkins, *Electron Spin Resonance in Liquids* (Plenum, New York, 1972).
[2]J. H. Freed, Ann. Rev. Phys. Chem. 23, 265 (1972).
[3]A. L. Kovarskii, A. M. Wasserman, and A. L. Buchachenko, J. Mag. Res. 7, 225 (1972).
[4]A. N. Kuznetsov and B. Ebert, Chem. Phys. Lett. 25, 342 (1974); A. N. Kuznetsov, A. Y. Volkov, V. A. Livshits, and A. T. Mirzoian, Chem. Phys. Lett. 26, 369 (1974).
[5]G. Feher, *Electron Paramagnetic Resonance* (Gordon and Breach, New York, 1970), pp. 109–118.
[6]V. B. Stryukov, P. A. Stunzhas, and S. T. Kirillov, Chem. Phys. Lett. 25, 453 (1974).
[7]I. C. P. Smith, in *Biological Applications of Electron Spin Resonance,* edited by H. M. Swartz, J. R. Bolton, and D. C. Borg (Wiley, New York, 1972), p. 483.
[8]P. C. Jost, A. S. Waggoner, and O. H. Griffith, in *Structure and Function of Biological Membranes,* edited by L. J. Rothfield (Academic, New York, 1972), p. 83.
[9]P. C. Jost and O. H. Griffith, in *Methods in Pharmacology: Vol. II. Physical Methods,* edited by C. Cheynell (Appleton-Century-Crofts, New York, 1971), p. 223.
[10]H. M. McConnell and B. G. McFarland, Quart. Rev. Biophys. 3, 91 (1970).
[11]B. H. Robinson, L. R. Dalton, L. A. Dalton, and A. L. Kwiram, Chem. Phys. Lett. 29, 56 (1974).
[12]J. S. Hyde and L. R. Dalton, Chem. Phys. Lett. 16, 568 (1972); L. R. Dalton, Bull. Am. Phys. Soc. 18, 1571 (1973).
[13]M. D. Smigel, L. R. Dalton, J. S. Hyde, and L. A. Dalton, Proc. Natl. Acad. Sci. USA 71, 1925 (1974).
[14]B. H. Robinson, J. L. Monge, L. A. Dalton, L. R. Dalton, and A. L. Kwiram, Chem. Phys. Lett. 28, 169 (1974); L. R. Dalton, P. W. Percival, and J. S. Hyde (unpublished).
[15]F. Francis, J. Chem. Soc., 2897 (1927).
[16]J. S. Hyde and D. D. Thomas, Annals N. Y. Acad. Sci. 222, 680 (1974); D. D. Thomas and H. M. McConnell, Chem. Phys. Lett. 25, 470 (1974); D. D. Thomas, J. S. Hyde, L. R. Dalton, and H. M. McConnell, J. Chem. Phys. (to be published).
[17]R. Karplus, Phys. Rev. 73, 1027 (1948).
[18]J. D. Macomber and J. S. Waugh, Phys. Rev. 140, A1494 (1965).